Journal of Materials Chemistry B

PAPER

Cite this: *J. Mater. Chem. B*, 2016, 4, 2253

Functionalized halloysite nanotube by chitosan grafting for drug delivery of curcumin to achieve enhanced anticancer efficacy†

Mingxian Liu,‡*[a] Yanzhou Chang,‡[b] Jing Yang,[a] Yuanyuan You,[b] Rui He,[a] Tianfeng Chen*[b] and Changren Zhou[a]

Received 23rd December 2015,
Accepted 27th February 2016

DOI: 10.1039/c5tb02725j

www.rsc.org/MaterialsB

Halloysite nanotubes (HNTs) have a unique tubular structure in nanoscale, and have shown potential as novel carriers for various drugs. Coating the nanotubes with a hydrophilic polymer shell can significantly decrease the toxicity and provide colloidal stability during blood circulation. Here, we synthesized chitosan grafted HNTs (HNTs-*g*-CS) and investigated their potential as a nano-formulation for the anticancer drug curcumin. The structure and properties of HNTs-*g*-CS were characterized using water contact angle, zeta-potential, Fourier transform infrared (FTIR) spectroscopy, thermogravimetric analysis (TGA), and transmission electron microscopy (TEM) techniques. HNTs-*g*-CS exhibit a maximum 90.8% entrapment efficiency and 3.4% loading capacity of curcumin, which are higher than those of raw HNTs. HNTs-*g*-CS also show no obvious hemolytic phenomenon and good stability in serum. The cumulative release ratio of curcumin from HNTs-*g*-CS/curcumin at cell lysate after 48 hours is 84.2%. The curcumin loaded HNTs-*g*-CS show specific toxicity to various cancer cell lines, including HepG2, MCF-7, SV-HUC-1, EJ, Caski and HeLa, and demonstrate an inhibition concentration of IC_{50} at 5.3–192 μM as assessed by cytotoxicity studies. The anticancer activity of this nanoformulation is extremely high in EJ cells compared with the other cancer cell lines. The cell uptake of HNTs-*g*-CS is confirmed by fluorescence microscopy. Flow cytometric analysis of curcumin loaded HNTs-*g*-CS shows that curcumin loaded HNTs-*g*-CS increase apoptosis on EJ cells. The content of ROS created by HNTs-*g*-CS/curcumin is more than that of free curcumin. All these results suggest that HNTs-*g*-CS are potential nanovehicles for anticancer drug delivery in cancer therapy.

1. Introduction

As shown in the World Cancer Report 2014, the worldwide burden of cancer in 2012 rose to an estimated 14 million new cases per year, a figure expected to rise to 22 million annually within the next two decades.[1] Over the same period, cancer deaths are predicted to rise from an estimated 8.2 million annually to 13 million per year. Therefore, searching for anticancer drugs is a hot topic at present. Curcumin (diferuloylmethane), a polyphenol derived from the root of the plant *Curcuma longa*, has been commonly used as a spice, flavoring agent, food preservative, coloring agent, or for decoration. There are extensive reports suggest that curcumin has great potential in the prevention and treatment of cancer.[2,3] The anticancer potential of curcumin mainly originates from its ability to suppress proliferation of a wide variety of tumor cells, down-regulate transcription factors (such as NF-κB, AP-1 and Egr-1), growth factor receptors (such as EGFR and HER2), necrosis factor, cell surface adhesion molecules, cyclin D1; and inhibit the activity of c-Jun N-terminal kinase, protein tyrosine kinases and protein serine/threonine kinases.[3] Additionally, curcumin can enhance wound healing, protect against liver injury, increase bile secretion, protect against cataract formation, protect against pulmonary toxicity and fibrosis, and is an anti-atherosclerotic.[3] However, low water solubility, poor bioavailability, easy degradation and metabolism, and the emergence of drug resistance in patients limit the practical application of curcumin for cancer therapy.[4,5] In previous reports, researchers have explored nanoscale drug delivery systems to improve the utilization and reduce the side effects of curcumin. Curcumin-loaded poly(lactide-*co*-glycolide) (PLGA) or polysaccharide nanoparticle formulations enhanced the cellular uptake of curcumin, and increased bioactivity *in vitro* and superior bioavailability *in vivo* over free curcumin.[6,7] Carbon nanomaterials[8,9] and

[a] *Department of Materials Science and Engineering, Jinan University, Guangzhou 510632, China. E-mail: liumx@jnu.edu.cn; Fax: +86 20-85223271; Tel: +86 20-85226663*
[b] *Department of Chemistry, Jinan University, Guangzhou 510632, China. E-mail: tchentf@jnu.edu.cn*

† Electronic supplementary information (ESI) available. See DOI: 10.1039/c5tb02725j

‡ The authors contributed equally to this work.

nanoclays[10,11] have also been used to load and slowly release curcumin. Very recently, Lazzara *et al.* prepared curcumin covalently grafted halloysite nanotubes (HNTs) as a dual-responsive prodrug for cancer therapy.[12] The nanoparticles exhibit high incorporation efficiencies of curcumin, which strongly enhance its anticancer efficacy compared with the free drug.

In comparison with other drug carriers, HNTs, naturally occurring inorganic clay nanotubes, have recently attracted significant attention in biomedical applications.[13–16] For drug delivery carrier applications, the advantages of HNTs include good particle dimensions (~50 nm outer diameter), numerous hydrophilic hydroxyl groups for functionalization, good stability in biological liquids, and low cost. HNTs have been successfully loaded with diverse active agents including pharmaceutical agents, antibacterials, corrosion inhibitors, mold growth inhibitors, genes, *etc*.[13,15,17,18] HNTs can entrap molecules *via* adsorption to the external and internal walls of the tubes or loading the drugs into the lumen and intercalation of substances between layers.[19] Release from the tube lumen typically lasts from several hours to days depending on the molecular weight, structure and solubility of the drugs in the release medium.[20] Also HNTs can be selectively functionalized on the inner and outer surfaces to load hydrophobic drugs and increase the dispersion ability in body fluids. Lvov *et al.* modified the surface groups of the tube lumen *via* grafting with octadecylphosphonic acid (ODP) and consecutively treated the outermost silica surface through silanization.[21] The ODP modified HNTs released 4 times more drugs compared with raw HNTs, indicating their higher adsorption capacity after functionalization. Coating the nanotubes with a hydrophilic polymer shell can significantly decrease the toxicity and provide colloidal stability during blood circulation.[22–24] Among the commercially available polymers, chitosan (CS) is a very useful reagent in biology because of its minimal toxicity, biocompatibility, protein resistance, good solubility in water, and biodegradability. A previous study showed that chitosan or polyethyleneimine (PEI) coated HNTs had additional delayed release effect for drugs compared with raw HNTs.[25] However, for these systems, only *in vitro* drug releasing experiments were performed.[11,26,27] Little is known at the cellular or animal level of their drug release behavior.

In this study, we proposed a new HNTs-based drug delivery system to improve the bioavailability of curcumin for cancer therapy. We modified HNTs with succinic anhydride to convert the surface hydroxyl groups to carboxyl groups, and then the HNTs–COOH were connected to biocompatible CS *via* *N*-(3-dimethylaminopropyl)-*N*′-ethylcarbodiimide (EDC)/*N*-hydroxysuccinimide (NHS) reaction, giving HNTs-*g*-CS (Fig. 1). The successful preparation of HNTs-*g*-CS was confirmed by various characterization methods. Afterwards, curcumin was loaded onto the surface of HNTs-*g*-CS through adsorption. The grafting of CS on HNTs can increase the hemocompatibility, stability in body fluids, the loading efficiency of curcumin, and the cytocompatibility. HNTs-*g*-CS act as a highly potent killer of various cancer cells *in vitro*, especially with a higher cytotoxicity to EJ human bladder cancer cell compared to free curcumin from the cell viability assay. The curcumin loaded HNTs-*g*-CS can also be taken up by cancer cells as confirmed by fluorescence microscopy. Therefore, the prepared HNTs-*g*-CS have potential applications as drug delivery systems in cancer therapy.

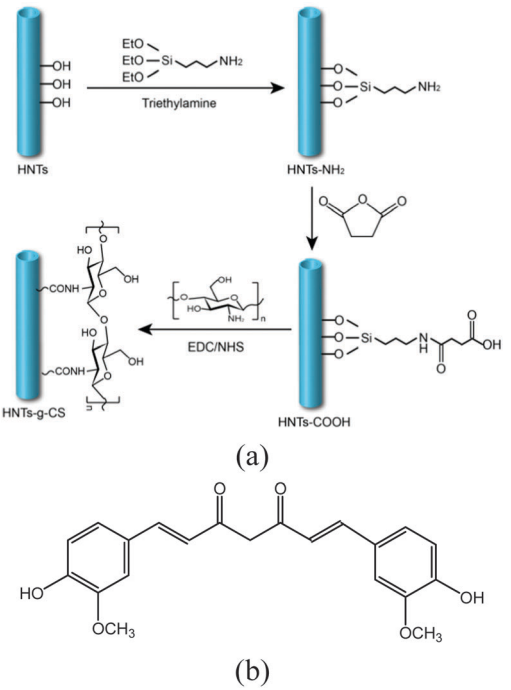

Fig. 1 Schematic illustration of the synthetic procedure for HNTs-*g*-CS (a) and the chemical structure of curcumin (b).

2. Experimental

2.1 Materials

Halloysite was purchased from Guangzhou Runwo Materials Technology Co., Ltd, China. Before use, halloysite was purified to remove the impurities according to ref. 28. The elemental composition of purified HNTs by X-ray fluorescence (XRF) was determined as follows (wt%): SiO_2, 54.29; Al_2O_3, 44.51; Fe_2O_3, 0.63; TiO_2, 0.006. The Brunauer–Emmett–Teller (BET) surface area of HNTs was 50.4 $m^2\ g^{-1}$. Chitosan (CS) powder was supplied by Jinan Haidebei Marine Bioengineering Co. Ltd, China. The deacetylation and viscosity-average molecular weight were 95% and 600 000 g mol^{-1}, respectively. Curcumin (Cur) with purity of 98% was obtained from Nanogong Sanxin Natural Pigment Ltd, China. Ultrapure water from a Milli-Q water system was used to prepare the aqueous solutions. 3-Aminopropyltriethoxy silane (APTES), trimethylamine (TEA), dimethyl formamide (DMF), *N*-(3-dimethylaminopropyl)-*N*′-ethylcarbodiimide (EDC) and *N*-hydroxysuccinimide (NHS) were purchased from Sigma-Aldrich. All other chemicals were used as purchased (Aladdin) without further purification.

2.2 Synthesize of the chitosan grafted HNTs (HNTs-*g*-CS)

CS grafted HNTs (HNTs-*g*-CS) were synthesized according to previous procedures with a slight modification.[29] Fig. 1 shows the synthesis procedure for HNTs-*g*-CS and the chemical

structure of curcumin. First, the surface hydroxyl groups of HNTs were transformed into amide groups by the grafting reactions with APTES in the presence of TEA as catalyst. Typically, 5 g HNTs were dispersed in 100 mL of toluene by sonication for 2 h and stirring (600 rpm) for 1 h. Afterward, 5 mL of TEA and 10 mL APTES were added to the HNTs suspension, and the mixture was stirred for 1 day at 80 °C under nitrogen atmosphere. The obtained HNTs–NH_2 were washed several times with DI water and ethanol, then collected, and dried at 50 °C under vacuum. HNTs–COOH were then synthesized from the HNTs–NH_2. 1 g succinic anhydride and 2.5 g HNTs–NH_2 powder were mixed in 90 mL dimethyl formamide (DMF), and the mixture was stirred at 25 °C for 1 day. The collected HNTs–COOH were dried in a vacuum oven at 50 °C. The obtained HNTs–COOH were added into 100 mL CS acidic solution (1 wt%) in the presence of EDC and NHS (weight ratio = 2/1) solution and stirred at room temperature for 24 h. Lastly, the resulting HNTs-*g*-CS were collected by centrifugation and vacuum dried at 50 °C.

2.3 Characterization

Water/toluene dispersion properties. The hydrophobicity of different HNTs sample was verified by extraction experiments.[30] About 0.2 g HNTs were added into 10 mL toluene followed by bath sonication for 10 min. After addition of 10 mL deionized water, the tubes were subjected to further bath sonication for 10 min. After standing, the observation of the retention of HNTs in the solvents was made. The amount of nanoparticles suspended in both solvents was estimated through the gravimetric method.[31] A quantitative analysis of the different HNTs dispersed in the oil (toluene) and the aqueous phases was calculated as the partition ratio (R):

$$R = \frac{W_{oil}}{W_{oil} + W_{aq}} \times 100\%$$

where W_{oil} and W_{aq} are the weight of the dispersed nanoparticles in the oil and the aqueous phases, respectively.

Water contact angle (WCA). WCAs of the samples were measured with a KRUSS drop shape analyzer DSA 100 instrument at 25.0 ± 0.1 °C for the support and the injecting syringe as well. Before determination, four different HNTs were pelleted using a universal tablet compression machine. The contact angle was measured just after water deposition onto the substrate. The water droplet volume was 6.0 ± 0.5 μL. Five measurements at least were carried out on each sample.

ζ-Potential analysis. Zeta potentials of the HNTs aqueous dispersions were measured using a Zetasizer Nano ZS (Malvern Ltd, UK). The concentration of the dispersions was 1×10^{-3} wt%. Prior to each measurement, the operating conditions were checked and adjusted using a calibrated latex dispersion supplied by the instrument manufacturer (zeta potential −50 ± 5 mV).

Fourier transform infrared spectroscopy (FTIR). The FTIR spectra of the samples were measured using a Bruker FTIR. Before measurement, HNTs were pelleted with potassium bromide. Thirty-two consecutive scans were taken and their average was recorded. Spectra were taken from 4000 to 400 cm^{-1}. The wavenumber resolution was 2 cm^{-1}.

Thermogravimetric analysis (TGA). TGA studies were carried out with a Mettler-Toledo TGA/DSC3+ from room temperature to 700 °C at a heating rate of 10 °C min^{-1} under N_2 atmosphere. This experiment was used to compare the thermal degradation behavior of the different HNTs. The percentage of grafting of HNTs was calculated using the following equation:

$$\text{Grafting ratio (\%)} = m_1/m_2 \times 100\%$$

where m_1 (g) is the weight of organics grafted onto HNTs, and m_2 (g) is the weight of HNTs.

Transmission electron microscopy (TEM). The dilute HNTs ethanol dispersions were dropped onto a carbon-film supported Cu grid and dried. Then the samples were observed using a Philips Tecnai 10 TEM under an accelerating voltage of 100 kV. In order to compare the diameter change of different HNTs, ImageJ software was used to measure the widths of 50 tubes from the TEM images.

2.4 Loading and *in vitro* delivery of curcumin by HNTs-*g*-CS nanocarrier

Encapsulating of curcumin by HNTs was performed by adapting the procedure described by Price *et al.*[32] Dispersed HNTs powders were mixed with 2 mg mL^{-1} solution of curcumin in ethanol as follows. 0.01 g HNTs, HNTs–NH_2, and HNTs-*g*-CS were each added to 10 mL deionized water. After ultrasonic dispersion, 100 μL, 200 μL, 500 μL curcumin ethanol solutions were added into the HNTs dispersions dropwise under continuous stirring for 60 min. Then the mixture solutions were separated by centrifugation at 4000 rpm for 10 min. The precipitates were washed twice with distilled water and then re-dispersed in ethanol. Yellow supernatant fluid was collected and quantified using a UV/Vis spectrophotometer at 420 nm.

$$\text{Entrapment efficiency (EE) (\%)} = \frac{\text{total amount of curcumin} - \text{free curcumin}}{\text{total amount of curcumin}} \times 100\%$$

$$\text{Loading efficiency (LE) (\%)} = \frac{\text{weight of loaded drug}}{\text{total weight of nanoparticles and loaded drug}} \times 100\%$$

In order to examine the curcumin release behavior, 0.005 g HNTs-*g*-CS/Cur nanoparticles were placed into 5 mL of releasing medium. The HNTs-*g*-CS/Cur was released at cell lysate and pH = 7.4 at 37 °C. At set time points, 200 μL of the solution was taken out to determine the release ratio using the ultraviolet spectrophotometer and the same volume of fresh buffer solution was replaced. The release ratio was calculated by comparing with the standard curves of curcumin in the corresponding medium (cell lysate and in PBS at pH = 7.4).

2.5 Hemocompatibility and stability of HNTs-*g*-CS

Human blood stabilized with heparin was kindly provided by the First Affiliated Hospital of Jinan University (Guangzhou, China). 5 mL fresh blood was added into 10 mL PBS solution, after

centrifuging the supernatant liquid was discarded. This procedure was repeated 3 times and the red blood cells (RBCs) were collected. Then, 320 μL the RBCs were added into 1680 μL PBS solution. 25 μL of the RBC suspension were further added into either 500 μL HNTs, HNTs-*g*-CS, HNTs-*g*-CS/Cur, or curcumin PBS solution with a concentration of 1 mg mL^{-1}. After gentle shaking the RBC suspension was incubated at 37 °C for 12 h. After incubation, all the samples were centrifuged at 1000*g* at 4 °C. 150 μL of the supernatant liquid was transferred into a 96-well plate. The hemolysis ratio was determined by measuring the absorbance at 570 nm using a microplate reader. The positive control group was 100% hemolysis (in ultrapure water) and the negative control group was 0% hemolysis (in PBS solution). The hemolysis ratio was calculated as follows:

$$\text{Hemolysis ratio } (\%) = \frac{\text{sample absorbance} - \text{negative control}}{\text{positive control} - \text{negative control}} \times 100\%$$

To examine the stability of the nanoparticles in biological fluids, 200 μL suspensions of HNTs and HNTs-*g*-CS were respectively dispersed into two media including 800 μL 10% FBS in DMEM and 800 μL serum. The changes of HNTs and HNTs-*g*-CS particle size were detected by a Nano-ZS instrument (Malvern Instrument Ltd) at different times. The hydrodynamic diameters were analyzed by cumulants. Samples were preserved at 4 °C in a refrigerator.

2.6 Cytotoxicity and cellular uptake of HNTs-*g*-CS/Cur

Cytocompatibility of the samples was assessed *via* the MTT method. Human cancer cell lines, including HepG2 hepatocellular carcinoma cells, MCF-7 breast adenocarcinoma cells, SV-HUC-1, EJ human bladder carcinoma cells, Caski human uterine cervical carcinoma cells and HeLa human uterine cervical carcinoma cells, were purchased from American Type Culture Collection (ATCC, Manassas, VA). The cells were cultured in DMEM medium with 10% fetal bovine serum, 100 units per mL penicillin and 50 units per mL streptomycin at 37 °C in a CO_2 incubator (95% relative humidity, 5% CO_2). Cell viability was determined by MTT assay as previously reported.[33]

Taking advantage of the intrinsic green fluorescence of curcumin, the cellular uptake of curcumin loaded HNTs-*g*-CS was examined by fluorescence microscopy. EJ human bladder carcinoma cells were grown in 96-well culture plates at 37 °C in a 5% CO_2 incubator up to 80% confluency. Cells were then treated with 4 μM HNTs-*g*-CS for 2, 4, 8 or 12 hours and analyzed for curcumin uptake. For microscopic analysis, cells were fixed using a fixative, washed three times with PBS, and analyzed under a fluorescence microscope (EVOS® FL Auto; Thermo Fisher Scientific Inc., USA).

2.7 *In vitro* cellular uptake of free curcumin and HNTs-*g*-CS/Cur

EJ cells were put into 96-well plates (10×10^3 cells per well). After 24 h, curcumin (4 μM) and HNTs-*g*-CS/Cur (4 μM) were added into the culture medium. At a specific point in time, the cells were washed with PBS to remove the extracellular nanoparticles. Then the cells were split with 100 mL of 0.1% Triton X-100 in NaOH solution. The intracellular amount of curcumin was measured using a UV-vis Reader at 426 nm wavelength (Spectra Max M5, Bio-Tek).

2.8 Flow cytometric analysis

Flow cytometry analysis was employed to examine the effects of the drugs on cell cycle distribution.[34] Briefly, cells (2×10^4 cells per mL) were separately treated with pure curcumin and HNTs-*g*-CS/Cur at different concentrations for 72 h. Cells were trypsinized after being washed with PBS three times. Subsequently, cells were fixed with 75% ethanol overnight at −20 °C. The fixed cells were stained with propidium iodide (PI) for about 1 hour in darkness. Finally the stained cells were measured with a Beckman Couler flow cytometer and the cell cycle distribution was analyzed with Multicycle software (Phoenix Flow Systems, San Diego, CA). For each experiment, 10 000 events per sample were recorded.

2.9 Production of intracellular reactive oxygen species (ROS)

ROS were detected using dihydroethidium (DHE) fluorescence assay as previously described.[35] EJ human bladder carcinoma cells (1×10^5 cells per mL) were seeded in a 2 cm Petri dish and allowed to be cultured for 12 h. After incubation with DHE for half an hour, cells were then treated with 20 μM free curcumin and HNTs-*g*-CS/Cur, respectively. A fluorescence microscope was utilized to visualize changes in fluorescence intensity.

3. Results and discussion

3.1 Synthesis of chitosan grafted HNTs (HNTs-*g*-CS)

We synthesized HNTs-*g*-CS by firstly treating HNTs–NH_2 with succinic anhydride to convert amide to carboxyl groups, and then HNTs–COOH were chemically connected to biocompatible chitosan by EDC/NHS coupling chemistry. The successful preparation of HNTs-*g*-CS was confirmed by water contact angle, zeta-potential, FTIR, TGA, and TEM investigations.

Fig. 2(a) shows the dispersion properties of HNTs with different surface groups in a toluene/water mixture. The top layer is toluene and the bottom is water. Due to the presence of hydroxyl groups on the surface of HNTs, they are hydrophilic and therefore located in the bottom layer of the toluene/water mixture. After grafting of amino groups by silylanization, the HNTs–NH_2 become hydrophobic as shown by their location in the toluene layer. The amide groups of HNTs–NH_2 further transform into carboxyl groups by reaction with succinic anhydride. As expected, HNTs–COOH exhibit hydrophilic properties as shown in Fig. 2(a). Lastly, the carboxyl groups of HNTs–COOH react with amide groups of CS, which results in amine ester bonds between HNTs and CS. Therefore, CS can be successfully grafted onto HNTs. The HNTs-*g*-CS show slightly hydrophobic properties as they are mainly located in the toluene layer. A quantitative analysis of the partition ratio (R) of the nanoparticles dispersed between the oil and the aqueous phases was performed. Fig. 2(b) shows that R values of raw HNTs and HNTs–COOH are 18.7 and 15.8, suggesting their hydrophilicity and oleophobicity. In contrast, the R values of HNTs–NH_2 and HNTs-*g*-CS are 79.1 and 76.7, suggesting their

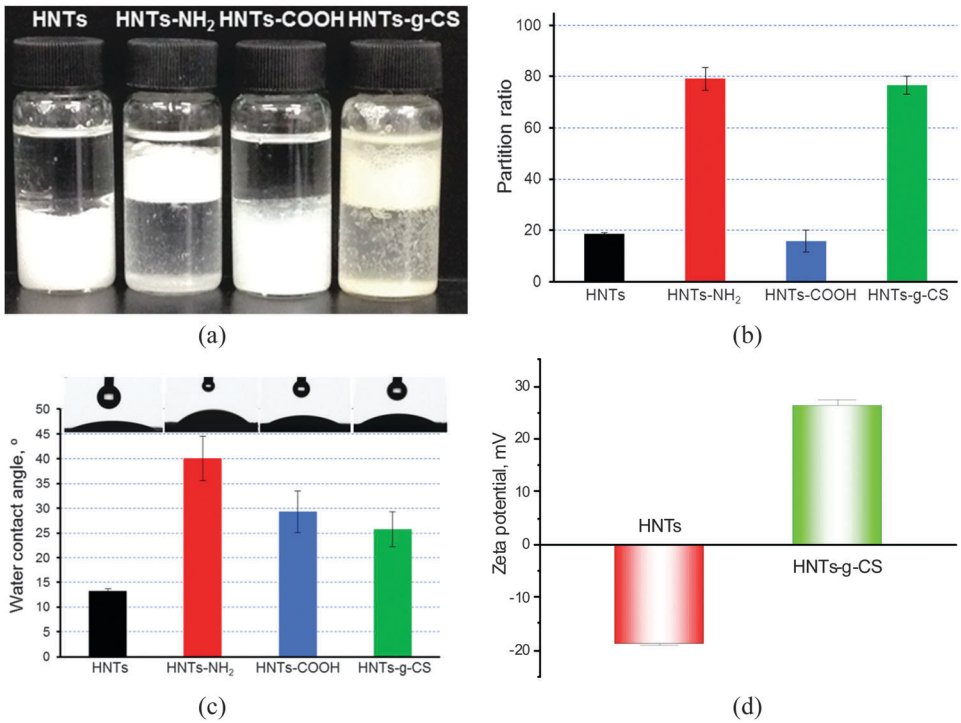

Fig. 2 The dispersion behaviour in a mixed toluene/water solution (a), partition ratio in the oil and the aqueous phases (b), the water contact angles (c), and the zeta potentials (d) of HNTs, HNTs–NH_2, HNTs–COOH, and HNTs-*g*-CS.

oleophilicity and hydrophobicity. Water contact angle experiments also confirmed the hydrophilic/hydrophobic properties of the four kinds of HNTs (Fig. 2(c)). Raw HNTs, HNTs–NH_2, HNTs–COOH, and HNTs-*g*-CS exhibit water contact angles of 12°, 40°, 29°, and 25°, respectively. Therefore, the grafting of CS on HNTs improves the hydrophobicity of the tubes, which facilitates the adsorption of hydrophobic anticancer drugs.

The successful grafting of CS on HNTs was further confirmed by zeta-potential measurements. HNTs are negatively charged with a zeta-potential of −20 mV (Fig. 2(d)). After grafting of CS, the HNTs-*g*-CS become positively charged with a zeta-potential of +25 mV. The presence of amino groups on the CS moiety endows HNTs with the positive charge,[36] enhancing the stability and cellular uptake of HNTs. This result again suggests that HNTs are chemically coated with positively charged CS.

The FT-IR technique was also employed to characterise the structure change of HNTs (Fig. 3). HNTs show typical absorption peaks around 3695, 3620, 1025 and 910 cm^{-1}, assigned to O–H stretching of inner-surface hydroxyl groups, O–H stretching of inner hydroxyl groups, in-plane Si–O stretching, and O–H deformation of inner hydroxyl groups, respectively.[37] After treatment with silane, the stretching peaks of NH_2 groups around 3486 cm^{-1} appear for the HNTs–NH_2 sample. The C–H bond stretching of silane is also seen in the range 2837–2987 cm^{-1}. Carbonyl vibrations of HNTs–COOH appear at 1565 and 1653 cm^{-1} for the amide and carboxylic acid groups, respectively. This is consistent with a previous report.[29] For the HNTs-*g*-CS sample, the peaks around 3450, 1657, 1567 and 1409 cm^{-1} are assigned to γO–H and C═O in amide groups (amide I band), NH-bending

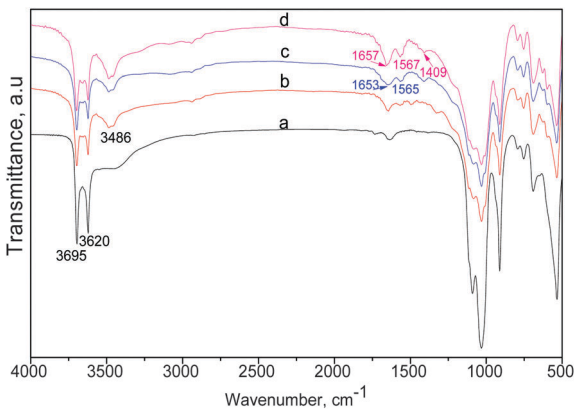

Fig. 3 FT-IR spectra of HNTs (a), HNTs–NH_2 (b), HNTs–COOH (c), and HNTs-*g*-CS (d).

vibration in amide groups, and deformation vibration of O–H for CS, respectively.[38,39] Therefore, from the FTIR results it is clear that CS is chemically grafted on HNTs.

TGA was conducted to compare the thermal stabilities of the different HNTs (Fig. 4). HNTs have a 17.4% weight loss at 700 °C. After grafting of silane, COOH, and CS, the weight loss at 700 °C of HNTs is 20.2%, 20.3%, and 25.7%, respectively. The grafting ratios of silane, COOH, and CS of HNTs are calculated as 3.39 wt%, 3.51 wt%, and 10.05 wt%, respectively. The high grafting percentage of CS is further confirmed by TEM images (Fig. 5). For raw HNTs, the tubes have smooth and uniform outer surfaces. A thick layer of CS covers the outer surfaces of

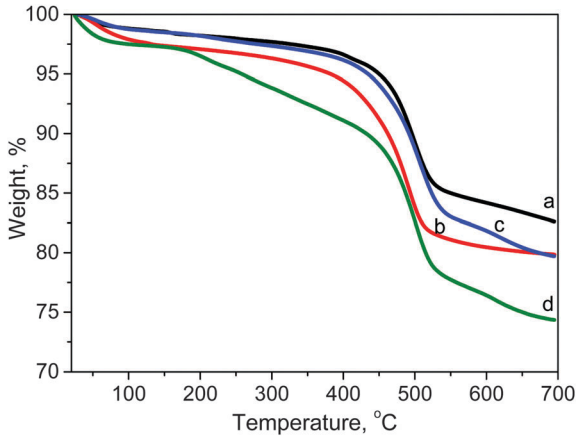

Fig. 4 TGA of HNTs (a), HNTs–NH_2 (b), HNTs–COOH (c), and HNTs-*g*-CS (d).

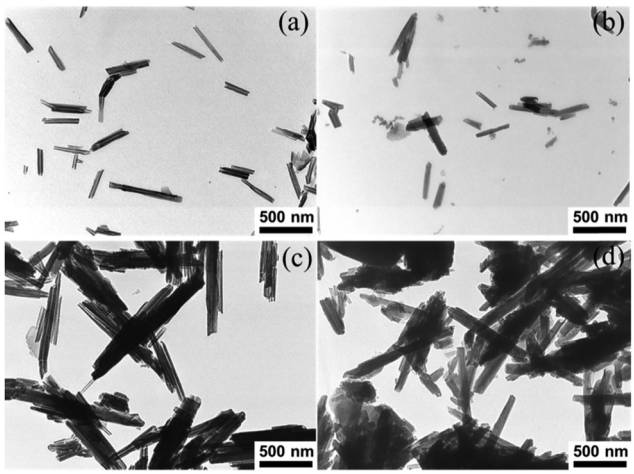

Fig. 5 TEM micrographs of HNTs (a), HNTs–NH_2 (b), HNTs–COOH (c), and HNTs-*g*-CS (d).

HNTs for the HNTs-*g*-CS sample. The tubes exhibit rough surface structures with increased diameter compared with the raw HNTs. The average diameter of HNTs-*g*-CS is 74.1 ± 22.3 nm, while the diameter of raw HNTs is 43.5 ± 18.5 nm. The grafting of CS on HNTs does not change the crystal structure of HNTs and the layer distance remains unchanged (Fig. S1, ESI†). All these results confirm the successful grafting of CS on the surface of HNTs.

3.2 Loading and release of curcumin from HNTs-*g*-CS nanocarrier

The entrapment (EE) and loading efficiencies (LE) of curcumin on the different HNTs were determined (Fig. 6). HNTs-*g*-CS exhibits maximum 90.8% EE and 3.4% LE of curcumin, which are higher than those of HNTs and HNTs–NH_2, further evidencing the important role of surface polymer grafting in determining the loading capability. The increased hydrophobicity and the surface roughness of the HNTs-*g*-CS are beneficial for the loading of curcumin. Both CS and HNTs are good carrier materials for drugs,[7,11] so there may be a synergic effect for loading of curcumin. The loading capacity of curcumin for all the HNTs increases with an increase in the ratio of curcumin and HNTs. From the FTIR results (Fig. S2, ESI†), the interactions between HNTs and curcumin may be totally physical adsorption, since no new peak or peak shift was found in the HNTs-*g*-CS/Cur.

The *in vitro* curcumin release from HNTs-*g*-CS/Cur was subsequently examined in PBS at pH 7.4 and cell lysate to simulate the normal body blood and tumor microenvironment at 37.4 °C. The resulting data are presented in Fig. 7. Curcumin is released slowly from HNTs-*g*-CS under pH 7.4 conditions. The release ratio after 48 hours for free curcumin from HNTs-*g*-CS/Cur is only 5.79%. After 144 hours, the release ratio reached only 32.46%. Subsequently, the release rate is up to 64.34% in 168 h. However, the release process of curcumin from HNTs-*g*-CS/Cur at cell lysate is much faster than that at pH 7.4. Its cumulative release rate reach 84.21% in 48 h. Thereafter, the cumulative release ratios of curcumin tend to be stable. Also, the release kinetics of curcumin from the HNTs-*g*-CS/Cur fit well with Ritger–Peppa's equation ($M_t/M_\infty = kt^n$, where M_t/M_∞ is the fractional amount of curcumin released at time t, k is a characteristic constant, and n is the release exponent, depending on the release mechanism and the geometry of the device[40]). The calculated constants n and k according to the fitted curves were 0.37 and 15.6 (R^2 is 0.78). The value of n is less than 0.45,

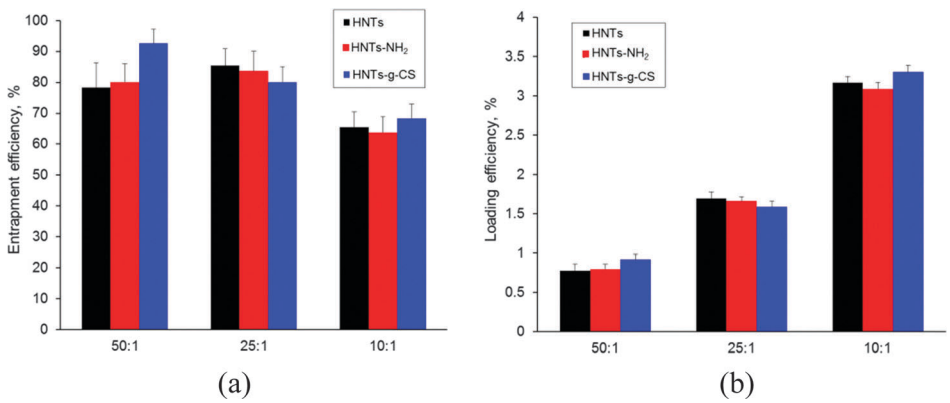

Fig. 6 The entrapment efficiency (a) and loading efficiency (b) for curcumin of different HNTs with different ratios of HNTs and curcumin.

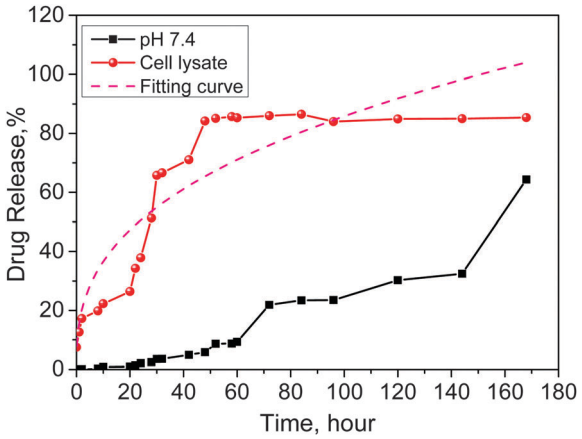

Fig. 7 Curcumin release curves from HNTs-*g*-CS/Cur in different media. The dashed line is the fitting curve of the curcumin release curve in cell lysate according to Ritger–Peppa's equation.

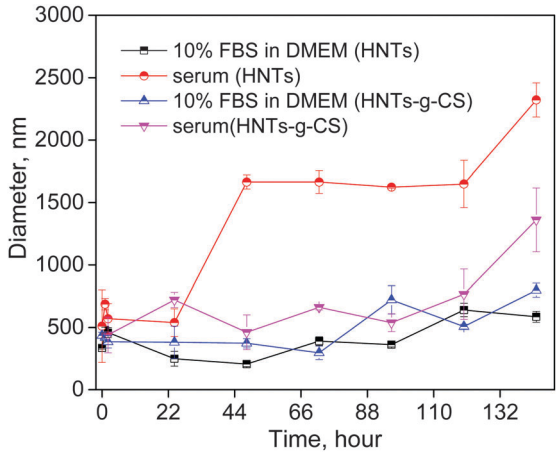

Fig. 9 The stabilities of HNTs and HNTs-*g*-CS in different media.

indicating the curcumin release follows the Fickian release behavior of swelling-controlled release systems from cylindrical particles.[41] Therefore, HNTs-*g*-CS can control the release of curcumin in the tumor microenvironment, while in blood and normal tissues the release ratio is low. These results demonstrate that HNTs-*g*-CS/Cur can realize sustained release and possibly show a long blood-circulation lifetime in the human body.

3.3 Hemocompatibility and stability of HNTs-*g*-CS in different liquid medium

Hemocompatibility of raw HNTs, curcumin, HNTs-*g*-CS, HNTs-*g*-CS/Cur was assessed by measuring the damage to human RBCs (Fig. 8). As expected, raw HNTs exhibit 100% lysis ratio due to their high concentration (1 mg mL^{-1}) and the unique needle-like morphology. The hemolysis of RBCs was also correlated with the interaction of the surface silanols of nanoparticles with endothelial and other normal cell membranes.[42] After grafting of CS, HNTs-*g*-CS show negligible hemolysis ratio. Free curcumin and HNTs-*g*-CS/Cur also have very low hemolysis ratios. These facts suggest that curcumin, HNTs-*g*-CS, and HNTs-*g*-CS/Cur are safe for intravenous injection. The inset photographs in Fig. 8 of the RBCs exposed to raw HNTs, curcumin and HNTs-*g*-CS, HNTs-*g*-CS/Cur also show that no obvious hemolytic phenomenon can be observed except the negative control (ultrapure water) and raw HNTs. Our data are different from the results of Zhao *et al.* who reported that HNTs did not show any hemolytic activity even at higher concentrations (2 mg mL^{-1}).[43] In another report, hemolysis increased with the content of graphene oxide (up to 96.0% at 0.5 mg mL^{-1}).[44] It was inferred that surface passivation of nanomaterials with bioagents will improve their biocompatibility.[45,46] Therefore, the prepared HNTs-*g*-CS can be used for different biological applications, such as vehicles for anticancer drug release.

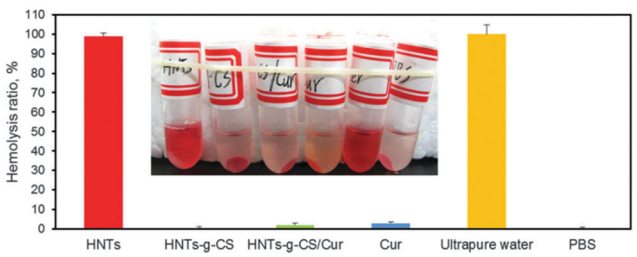

Fig. 8 *In vitro* hemocompatibility assay of HNTs, HNTs-*g*-CS, HNTs-*g*-CS/Cur, Cur, the positive control (ultrapure water, 100% lysis), and negative control (PBS, 0% lysis).

The stabilities of raw HNTs and HNTs-*g*-CS in different liquids were investigated (Fig. 9). For all the nanoparticles, the diameter increases with the incubation time, which is attributed to the aggregation of the nanoparticles. In DMEM solution (10% FBS), a very slight increase of the diameter for both raw HNTs and HNTs-*g*-CS is found. This is attributed to the increased stability of the tubes in the DMEM solution containing FBS, caused by the protein adsorption on the tube surfaces. Interestingly, compared with raw HNTs, the HNTs-*g*-CS show a significant increase in stability of the tubes in the serum. This is also attributed to the improved biocompatibility of HNTs caused by the grafting of CS. The increased stability in the serum is beneficial for the application of the nanocarriers in injection administration in cancer therapy.

3.4 Cytotoxicity and cellular uptake of HNTs-*g*-CS/Cur nanoformulation

Curcumin can suppress the proliferation and induce apoptosis of a wide variety of tumor cells.[3] However, the bioavailability of free curcumin is low. This study aimed to use HNTs-*g*-CS as a nanocarrier of curcumin to overcome the drawbacks of low aqueous solubility, difficulty in penetrating the cell membrane, and low biocompatibility of curcumin. The effects of HNTs, Cur and HNTs-*g*-CS/Cur on a series of cancer cells were evaluated by MTT method. As shown in Table 1, raw HNTs do not show any anticancer activities against EJ human bladder carcinoma (Fig. S3, ESI†), MCF-7 breast adenocarcinoma, SV-HUC-1, HepG2 hepatocellular carcinoma and Caski human uterine cervical carcinoma cells. Also, raw HNTs show good cytocompatibility towards L02 human normal liver cells and NIH-3T3 mouse

Table 1 IC_{50} data of curcumin, HNTs, and HNTs-*g*-CS/Cur for different tumor cells and normal cells

Sample	IC_{50}						
	SV-HUC-1	EJ	Caski	HepG-2	HeLa	L02	NIH-3T3
HNTs ($\mu g\ mL^{-1}$)	>700	>700	>700	>700	>700	>700	>700
Cur (μM)	95	30	100	16	80	>160	80
HNTs-*g*-CS/Cur (μM)	85	5.3	>64	>64	>64	>192	>192

embryonic fibroblast cells. The IC_{50} data of the cancer cells and the normal cells treated with curcumin are low, suggesting the high cytotoxicity of curcumin. Also, curcumin induces cell apoptosis depending on the cell type. The HNTs-*g*-CS/Cur nanoformulation also shows high toxicity towards cancer cells. For example, EJ cells display the highest sensitivity to HNTs-*g*-CS/Cur with an IC_{50} value of 5.3 μM. The present result is consistent with previous reported HNTs based anticancer drug delivery systems.[47]

Fig. 10 demonstrates the EJ cell morphology treated with curcumin and HNTs-*g*-CS/Cur for 3 days. Consistent with the previous results, the cells in the control and raw HNTs groups show normal cell morphology (Fig. S4, ESI†), while the free curcumin and HNTs-*g*-CS/Cur groups show cell morphology with round or irregular shapes indicating the dead state of the cells. Especially for the HNTs-*g*-CS/Cur groups, almost no living cells can be identified in the visual field. Therefore, the high killing ability towards cancer cells for HNTs-*g*-CS/Cur suggests HNTs-*g*-CS can potentially be used as anticancer drug carriers.

Taking advantage of the autofluorescence properties of curcumin, the intracellular uptake of curcumin loaded HNTs-*g*-CS nanoparticles was observed by fluorescence microscopy. Hoechst fluorescence probe was used to stain the nuclei. As presented in Fig. 11(a), HNTs began to enter the cell membrane at 2 h, entered into the cells at 4 h, and the cytoplasm was filled at 8 h. It was clearly observed that the cells treated with HNTs-*g*-CS/Cur showed profound fluorescence intensity in plasma at 12 h. According to these fluorescence images, we speculated that the observed higher uptake of HNTs might be due to lysosome-mediated endocytosis, which has already been found in other systems.[34,48] In addition, we quantified the cellular uptake of free

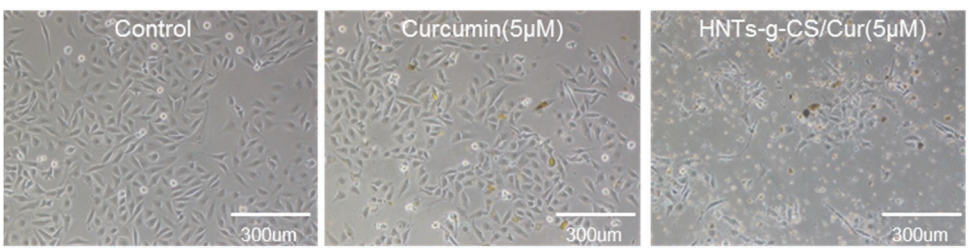

Fig. 10 Cell morphology of EJ after culture for 3 days for different samples as indicated.

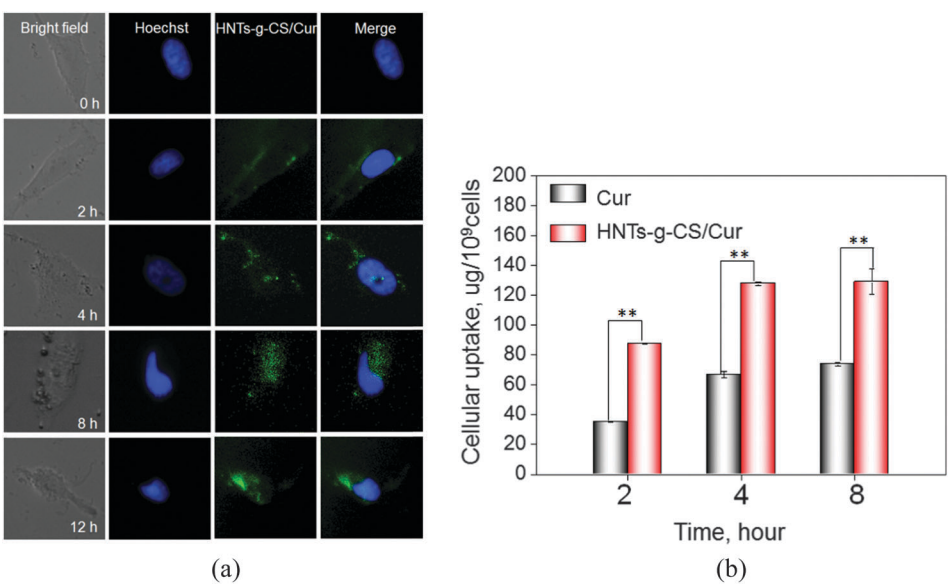

Fig. 11 (a) Intracellular localization of HNTs-*g*-CS/Cur. Colocalization of HNTs-*g*-CS/Cur (green fluorescence), nucleus (blue fluorescence) in EJ cells. The cells were treated with HNTs-*g*-CS/Cur (20 μM) for different periods of time and visualized under a fluorescence microscope. (b) Quantitative cellular uptake of free curcumin and HNTs-*g*-CS/Cur in EJ (2×10^5 cells per mL). EJ cells were treated with free curcumin (4 μM) and HNTs-*g*-CS/Cur (4 μM) for different periods of time.

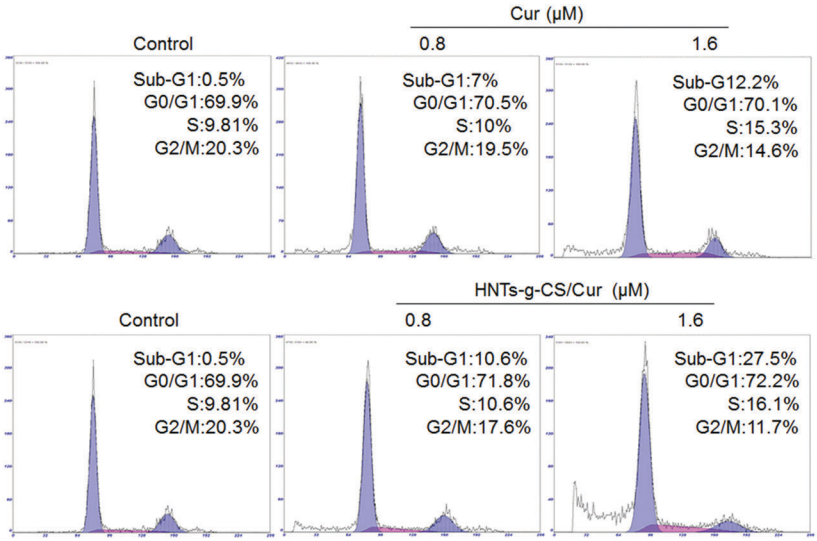

Fig. 12 Flow cytometric analysis of free curcumin and HNTs-*g*-CS/Cur in EJ cells for 72 h.

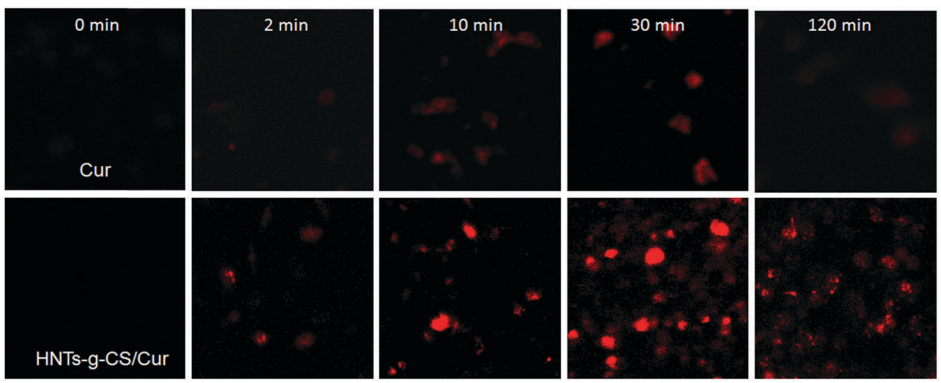

Fig. 13 The fluorescent ROS in EJ cells (1×10^5 cells per mL) after exposure to free curcumin and HNTs-*g*-CS/Cur (20 μM) for different periods of time.

curcumin and HNTs-*g*-CS/Cur in 2 h, 4 h and 8 h (Fig. 11(b)). It was found that the intracellular concentrations of HNTs-*g*-CS/Cur were much higher than those of free curcumin. For instance, the intracellular concentrations of free curcumin and HNTs-*g*-CS/Cur were 70 μg per 10^9 cells and 134 μg per 10^9 cells after 4 h incubation, respectively. These results suggested that HNTs-*g*-CS/Cur had a higher cellular uptake. Therefore, this result certifies that HNTs-*g*-CS is effective in the enhancement of uptake of curcumin. A previous report also found that the cellular uptake of curcumin could be greatly improved by encapsulating curcumin in CS/poly(ε-caprolactone) (PCL) or monomethoxy poly(ethylene glycol) (MPEG)–PCL polymer in cancer cells.[7,49,50] In brief, HNTs-*g*-CS nanoparticles can also be a good curcumin delivery platform with simultaneous therapy as well as imaging characteristics for cancer cells.

In order to investigate the underlying mechanisms for the cell death induced by Cur and HNTs-*g*-CS/Cur, PI staining followed by flow cytometric analysis was used to determine the cell cycle in the treated cells.[51] As shown in Fig. 12, both free curcumin and HNTs-*g*-CS/Cur can induce mild cell cycle arrest and apoptosis of EJ in a dose-dependent way, as reflected by the increase in G0/G1 and Sub-G1 peaks. For example, the cells in the Sub-G1 phase were distinctly increased to 10.6% and 27.5% after 72 h treatment with 0.8 and 1.6 μM HNTs-*g*-CS/Cur. By contrast, the activity of free curcumin was much lower than that of HNTs-*g*-CS/Cur. These results indicated that curcumin loaded HNTs-*g*-CS can greatly improve the anti-tumor activity.

A previous study found that reactive oxygen species (ROS) play an important role in eliciting cell apoptosis.[52] Free radicals can be reduced by dihydroethidium (DHE) probe to generate substances that can be combined with RNA or DNA to produce red fluorescence. The fluorescence intensity was determined using a fluorescence microscope. As shown in Fig. 13, the fluorescence intensity induced by free curcumin and HNTs-*g*-CS/Cur have a common trend which changes from dark to bright and then gradually dims in 0 to 120 minutes. However, the fluorescence intensity induced by HNTs-*g*-CS/Cur is much brighter and more durable than that by free curcumin. The content of ROS generated by HNTs-*g*-CS/Cur is higher than that of free curcumin. Therefore, curcumin loaded HNTs-*g*-CS could exhibit significantly improved antitumor activity.

4. Conclusions

HNTs with a unique tubular structure in nanoscale have been found to be novel nanocarriers for the anticancer drug curcumin. Coating the nanotubes with CS can significantly decrease the toxicity and provide colloidal stability. Water contact angle, zeta-potential, FT-IR spectroscopy, XRD, TGA, and TEM techniques confirm the grafting of CS on HNTs. HNTs-*g*-CS exhibit a maximum 90.8% EE and 3.4% loading capacity of curcumin, which are higher than thoe of HNTs. The *in vitro* release process of curcumin from HNTs-*g*-CS/Cur at cell lysate is much faster than that at pH 7.4. The HNTs-*g*-CS show improved hemocompatibility and stability. The curcumin loaded HNTs-*g*-CS show specific toxicity towards cancer cells, especially for the EJ cells. Fluorescence microscopy results show that HNTs-*g*-CS can be taken up by cancer cells. Flow cytometric analysis of curcumin loaded HNTs-*g*-CS show increased apoptosis on EJ cells. The content of ROS which is created by HNTs-*g*-CS/Cur is more than that of free curcumin. These results indicate that HNTs-*g*-CS can be a potential nanovehicle for curcumin to achieve enhanced anticancer efficacy.

Acknowledgements

This work was financially supported by National High Technology Research and Development Program of China (2015AA020915 and SS2014AA020538), the National Natural Science Foundation of China (grant no. 51473069 and 51502113), the Guangdong Natural Science Funds for Distinguished Young Scholar (grant no. S2013050014606 and S2013050014667), and the Fundamental Research Funds for the Central Universities (21615204).

References

1 B. W. Stewart and C. P. Wild, World Cancer Report 2014, IARC Nonserial Publication, 2014.
2 A.-L. Cheng, C.-H. Hsu, J.-K. Lin, M.-M. Hsu, Y.-F. Ho, T.-S. Shen, J.-Y. Ko, J.-T. Lin, B.-R. Lin and W. Ming-Shiang, *Anticancer Res.*, 2000, **21**, 2895–2900.
3 B. B. Aggarwal, A. Kumar and A. C. Bharti, *Anticancer Res.*, 2003, **23**, 363–398.
4 M. M. Yallapu, M. Jaggi and S. C. Chauhan, *Drug Discovery Today*, 2012, **17**, 71–80.
5 P. Anand, A. B. Kunnumakkara, R. A. Newman and B. B. Aggarwal, *Mol. Pharmaceutics*, 2007, **4**, 807–818.
6 P. Anand, H. B. Nair, B. Sung, A. B. Kunnumakkara, V. R. Yadav, R. R. Tekmal and B. B. Aggarwal, *Biochem. Pharmacol.*, 2010, **79**, 330–338.
7 F. Akhtar, M. M. A. Rizvi and S. K. Kar, *Biotechnol. Adv.*, 2012, **30**, 310–320.
8 H. Li, N. Zhang, Y. Hao, Y. Wang, S. Jia, H. Zhang, Y. Zhang and Z. Zhang, *Drug Delivery*, 2014, **21**, 379–387.
9 C.-W. Liu, F. Xiong, H.-Z. Jia, X.-L. Wang, H. Cheng, Y.-H. Sun, X.-Z. Zhang, R.-X. Zhuo and J. Feng, *Biomacromolecules*, 2013, **14**, 358–366.
10 M. Massaro, S. Riela, P. Lo Meo, R. Noto, G. Cavallaro, S. Milioto and G. Lazzara, *J. Mater. Chem. B*, 2014, **2**, 7732–7738.
11 S. Riela, M. Massaro, C. G. Colletti, A. Bommarito, C. Giordano, S. Milioto, R. Noto, P. Poma and G. Lazzara, *Int. J. Pharm.*, 2014, **475**, 613–623.
12 M. Massaro, R. Amorati, G. Cavallaro, S. Guernelli, G. Lazzara, S. Milioto, R. Noto, P. Poma and S. Riela, *Colloids Surf., B*, 2016, **140**, 505–513.
13 Y. Lvov and E. Abdullayev, *Prog. Polym. Sci.*, 2013, **38**, 1690–1719.
14 M. Liu, Z. Jia, D. Jia and C. Zhou, *Prog. Polym. Sci.*, 2014, **39**, 1498–1525.
15 Y. Lvov, W. Wang, L. Zhang and R. Fakhrullin, *Adv. Mater.*, 2016, **28**, 1227–1250.
16 L. He, H. Lai and T. Chen, *Biomaterials*, 2015, **51**, 30–42.
17 J. Xue, Y. Niu, M. Gong, R. Shi, D. Chen, L. Zhang and Y. Lvov, *ACS Nano*, 2015, **9**, 1600–1612.
18 M. Massaro, S. Piana, C. G. Colletti, R. Noto, S. Riela, C. Baiamonte, C. Giordano, G. Pizzolanti, G. Cavallaro, S. Milioto and G. Lazzara, *J. Mater. Chem. B*, 2015, **3**, 4074–4081.
19 Y. Fu, D. Zhao, P. Yao, W. Wang, L. Zhang and Y. Lvov, *ACS Appl. Mater. Interfaces*, 2015, **7**, 8156–8165.
20 P. Lo Meo, *J. Mater. Chem. B*, 2014, **2**, 7732–7738.
21 W. O. Yah, A. Takahara and Y. M. Lvov, *J. Am. Chem. Soc.*, 2012, **134**, 1853–1859.
22 P. D. Thornton and A. Heise, *J. Am. Chem. Soc.*, 2010, **132**, 2024–2028.
23 Y. Zhang, M. Wang, Y.-g. Zheng, H. Tan, B. Y.-w. Hsu, Z.-c. Yang, S. Y. Wong, A. Y.-c. Chang, M. Choolani, X. Li and J. Wang, *Chem. Mater.*, 2013, **25**, 2976–2985.
24 L. He, T. Chen, Y. You, H. Hu, W. Zheng, W.-l. Kwong, T. Zou and C.-M. Che, *Angew. Chem., Int. Ed.*, 2014, **53**, 12532–12536.
25 S. R. Levis and P. B. Deasy, *Int. J. Pharm.*, 2003, **253**, 145–157.
26 M. Massaro, C. G. Colletti, R. Noto, S. Riela, P. Poma, S. Guernelli, F. Parisi, S. Milioto and G. Lazzara, *Int. J. Pharm.*, 2015, **478**, 476–485.
27 G. Cavallaro, G. Lazzara, M. Massaro, S. Milioto, R. Noto, F. Parisi and S. Riela, *J. Phys. Chem. C*, 2015, **119**, 8944–8951.
28 M. Liu, B. Guo, Q. Zou, M. Du and D. Jia, *Nanotechnology*, 2008, **19**, 205709.
29 Y. Joo, Y. Jeon, S. U. Lee, J. H. Sim, J. Ryu, S. Lee, H. Lee and D. Sohn, *J. Phys. Chem. C*, 2012, **116**, 18230–18235.
30 B. Guo, Q. Zou, Y. Lei and D. Jia, *Polym. J.*, 2009, **41**, 835–842.
31 G. Cavallaro, G. Lazzara, S. Milioto and F. Parisi, *Langmuir*, 2015, **31**, 7472–7478.
32 R. R. Price, B. P. Gaber and Y. Lvov, *J. Microencapsulation*, 2001, **18**, 713–722.
33 H. Lai, Z. Zhao, L. Li, W. Zheng and T. Chen, *Metallomics*, 2015, **7**, 439–447.
34 Z. Darzynkiewicz and H. Zhao, *eLS*, 2014, DOI: 10.1002/9780470015902.a9780470002571.pub9780470015902.
35 Y. Liu, Y. Luo, X. Li, W. Zheng and T. Chen, *Chem. – Asian J.*, 2015, **10**, 642–652.
36 M. Liu, Y. Zhang, C. Wu, S. Xiong and C. Zhou, *Int. J. Biol. Macromol.*, 2012, **51**, 566–575.

37 P. Yuan, P. D. Southon, Z. Liu, M. E. R. Green, J. M. Hook, S. J. Antill and C. J. Kepert, *J. Phys. Chem. C*, 2008, **112**, 15742–15751.
38 M. L. Duarte, M. C. Ferreira, M. R. Marvao and J. Rocha, *Int. J. Biol. Macromol.*, 2002, **31**, 1–8.
39 A. Pawlak and M. Mucha, *Thermochim. Acta*, 2003, **396**, 153–166.
40 P. L. Ritger and N. A. Peppas, *J. Controlled Release*, 1987, **5**, 23–36.
41 P. L. Ritger and N. A. Peppas, *J. Controlled Release*, 1987, **5**, 37–42.
42 Y.-S. Lin and C. L. Haynes, *J. Am. Chem. Soc.*, 2010, **132**, 4834–4842.
43 Y. Zhao, S. Wang, Q. Guo, M. Shen and X. Shi, *J. Appl. Polym. Sci.*, 2013, **127**, 4825–4832.
44 R. Feng, Y. Yu, C. Shen, Y. Jiao and C. Zhou, *J. Biomed. Mater. Res., Part A*, 2015, **103**, 2006–2014.
45 M. M. van Schooneveld, E. Vucic, R. Koole, Y. Zhou, J. Stocks, D. P. Cormode, C. Y. Tang, R. E. Gordon, K. Nicolay, A. Meijerink, Z. A. Fayad and W. J. M. Mulder, *Nano Lett.*, 2008, **8**, 2517–2525.
46 Y. Zhang, Y. Bai and B. Yan, *Drug Discovery Today*, 2010, **15**, 428–435.
47 M. R. Dzamukova, E. A. Naumenko, Y. M. Lvov and R. F. Fakhrullin, *Sci. Rep.*, 2015, **5**, 10560.
48 A. Sahu, N. Kasoju and U. Bora, *Biomacromolecules*, 2008, **9**, 2905–2912.
49 J. Liu, L. Xu, C. Liu, D. Zhang, S. Wang, Z. Deng, W. Lou, H. Xu, Q. Bai and J. Ma, *Carbohydr. Polym.*, 2012, **90**, 16–22.
50 C. Mohanty and S. K. Sahoo, *Biomaterials*, 2010, **31**, 6597–6611.
51 T. Chen, Y. Liu, W. J. Zheng, J. Liu and Y. S. Wong, *Inorg. Chem.*, 2010, **49**, 6366–6368.
52 L. Li, Y.-S. Wong, T. Chen, C. Fan and W. Zheng, *Dalton Trans.*, 2012, **41**, 1138–1141.